doi:10.1006/jmbi.2001.5077 available online at http://www.idealibrary.com on IDEAL® *J. Mol. Biol.* (2001) **313**, 1045–1057

JMB

Refined Structure of αβ-Tubulin at 3.5 Å Resolution

J. Löwe[1], H. Li[2], K. H. Downing[2] and E. Nogales[2,3]*

[1]*MRC Laboratory of Molecular Biology, Cambridge, UK*

[2]*Life Science Division, Lawrence Berkeley Natl. Lab. Berkeley, CA 94720 USA*

[3]*Howard Hughes Medical Institute, UC Berkeley Berkeley, CA 94720-3200 USA*

**Corresponding author*

We present a refined model of the αβ-tubulin dimer to 3.5 Å resolution. An improved experimental density for the zinc-induced tubulin sheets was obtained by adding 114 electron diffraction patterns at 40-60° tilt and increasing the completeness of structure factor amplitudes to 84.7%. The refined structure was obtained using maximum-likelihood including phase information from experimental images, and simulated annealing Cartesian refinement to an *R*-factor of 23.2 and free *R*-factor of 29.7. The current model includes residues α:2-34, α:61-439, β:2-437, one molecule of GTP, one of GDP, and one of taxol, as well as one magnesium ion at the non-exchangeable nucleotide site, and one putative zinc ion near the M-loop in the α-tubulin subunit. The acidic C-terminal tails could not be traced accurately, neither could the N-terminal loop including residues 35-60 in the α-subunit. There are no major changes in the overall fold of tubulin with respect to the previous structure, testifying to the quality of the initial experimental phases. The overall geometry of the model is, however, greatly improved, and the position of side-chains, especially those of exposed polar/charged groups, is much better defined. Three short protein sequence frame shifts were detected with respect to the non-refined structure. In light of the new model we discuss details of the tubulin structure such as nucleotide and taxol binding sites, lateral contacts in zinc-sheets, and the significance of the location of highly conserved residues.

© 2001 Academic Press

Keywords: tubulin; taxol; zinc-sheets; electron crystallography; crystallographic refinement

Introduction

Microtubules are cytoskeletal polymers essential in all eukaryotic cells, with functions extending from cellular transport to cell motility and mitosis.[1] They are made of repeating αβ-tubulin heterodimers that bind head to tail into protofilaments. About 13 of these protofilaments associate in parallel making the microtubule wall, and giving rise to a polymer with a well defined polarity. Essential to the function of microtubules is their ability to switch stochastically between growing and shrinking phases (dynamic instability),[2] a non-equilibrium behavior of tubulin that is based on nucleotide binding and hydrolysis. Each tubulin monomer binds one molecule of GTP. The nucleotide bound to α-tubulin, at the so called N-site, is non-exchangeable. The nucleotide bound to β-tubulin, at the E-site, is exchangeable. GTP is required at the E-site in order for tubulin to polymerize,[3] but this nucleotide is hydrolyzed and becomes non-exchangeable upon polymerization. The resulting metastable microtubule structure is thought to be stabilized by a cap of remaining GTP-tubulin subunits at the ends, the loss of which results in rapid depolymerization.

The structure of the tubulin dimer was obtained by electron crystallography of zinc-induced tubulin sheets,[4] which are formed by the antiparallel association of protofilaments. Addition of taxol stabilized the sheets against cold temperature depolymerization and aging,[5] similar to the effects of taxol on microtubules. Using low-dose methods, cryo-preservation and image processing, a structure of the tubulin dimer bound to taxol was obtained at 3.7 Å resolution that included all but the last acidic C-terminal residues. Each compact monomer contains an N-terminal, nucleotide-binding domain, comprising six parallel β-strands (S1-S6) alternating with helices (H1-H6). The loops joining each strand with the beginning of the next helix are directly involved in binding the nucleotide (loops T1-T6). Within each monomer, nucleotide binding is completed by interaction with the

E-mail address of the corresponding author: enogales@lbl.gov

0022-2836/01/051045–13 $35.00/0

© 2001 Academic Press

N-terminal end of the core helix H7. The core helix connects the nucleotide binding domain with the smaller, second domain, formed by three helices (H8-H10) and a mixed beta sheet (S7-S10). The C-terminal region is formed by two antiparallel helices (H11-H12) that cross over the previous two domains. The N-site GTP in α-tubulin is buried at the monomer-monomer interface within the dimer, while the GDP at the E-site is exposed on the surface of the dimer, thus explaining the exchangeability of the nucleotides.

The longitudinal contact between subunits, very similar between monomers within the dimer and between dimers, is very extensive (about 3000 Å^2 are buried with the formation of the dimer from the monomers, or in the contact between dimers).[6,7] The two surfaces involved in the interfaces are convoluted in shape and highly complementary. About 52% of the residues at the intradimer interface are totally conserved across species, while about 40% are conserved at the interdimer contact.[8] Upon polymerization the E-site nucleotide becomes buried at the newly formed interface. Loop T7, a region in the tubulin structure opposed to the nucleotide site, is involved in the interaction with the nucleotide in the next subunit along the protofilament.[6] T7 includes highly conserved residues in both tubulin subunits (GXXNXD). This conservation extends to their bacterial homologue FtsZ.[6,9] The interaction with the nucleotide across the longitudinal interface is completed by Lys254 in β-tubulin (within the H8 helix), which interacts with the γ-phosphate of the N-site nucleotide, and in α-tubulin by Glu254, which is in a position that would be close to the γ-phosphate of the E-site nucleotide (in the crystal structure this nucleotide is GDP after hydrolysis during the formation of the sheets). The corresponding aspartic acid in FtsZ has been shown to be required for nucleotide hydrolysis,[10] supporting the idea that α: Glu254 is essential for the polymerization-dependent hydrolysis. In yeast TUB1 mutation of Asp251 and Glu254 to alanine residues results in a dominant lethal phenotype.[11] Each mutation on its own is a dominant lethal, and transient expression of the mutant α-tubulins results in hyperstable microtubules (K. Anders and D. Botstein, personal communication), in further agreement with the requirement of these residues for nucleotide hydrolysis.

A high resolution model of the microtubule was obtained by docking the crystal structure of the tubulin protofilament into a reconstruction of the microtubule obtained by cryo-electron microscopy and helical image reconstruction.[7] The plus end of the microtubule is crowned by β-tubulin subunits exposing their nucleotide surface to the solution, while the minus end is crowned by α-subunits exposing their catalytic end. This orientation has very important repercussions for the GTP-cap model of microtubule dynamics.[8]

The docking showed that the C-terminal helices form the crest of the protofilaments on the outside surface of the microtubule. The bumpy inside surface of the microtubule is defined by a series of loops: loops H1-S2 and H2-S3, which were poorly resolved in the original crystal structure of the sheets; and the S9-S10 loop, which is eight residues longer in α-tubulin and in β-tubulin forms part of the taxol binding site. The docking indicates that the lateral contact between protofilaments is dominated by the interaction of the M-loop, the loop between S7 and H9, with loop H1-S2 and helix H3. This interaction, in comparison with the longitudinal contact, has an important ionic contribution, both for α-α and β-β contacts. The M-loop is in a position where it could hinge without disrupting its interaction with the adjacent subunit, thereby allowing for the known variability in protofilament number of reconstituted microtubules. The sequence of this loop corresponds to one of the most divergent segments between α and β-tubulins. In β-tubulin the M-loop is an essential part of the taxol binding pocket, while H3 follows loop T3, which is involved in binding the γ-phosphate of the E-site nucleotide. The conformation of the M-loop is stabilized in the α-subunit by the long S9-S10 loop. In the β-subunit a similar stabilizing function may be played by taxol and taxol-like compounds.[12] On the other hand, the destabilizing effect of nucleotide hydrolysis may be due to a conformational change transmitted to H3 through the γ-phosphate sensing loop.

Here we present a refined model of the αβ-tubulin dimer to 3.5 Å resolution, carried out using standard X-ray crystallography methodology. The new structural model is very similar to that originally published but has much improved geometry, better defined side-chain conformations and includes three protein sequence frame shifts of one residue in both α and β-tubulins. Assignments were made for a magnesium ion in the non-exchangeable site, and a zinc ion at the lateral contact between α subunits. We discuss in detail the lateral contacts in zinc-sheets and the nucleotide and taxol binding sites.

Results

Previous to the refinement the data set was improved by incorporating 114 additional diffraction patterns. A few of the patterns extend to 2.5 Å. However the completeness at this resolution is very low. In the resolution shell from 3.7 to 3.5 Å the completeness dropped to 83.7%, which we considered the lower limit for this work. The overall $I/(\sigma I)$ for this data set was 5.4, 2.3 for the last resolution shell (3.7-3.5 Å). The overall multiplicity was 6. No attempt has been made to correct for multiple scattering and diffuse scattering as was previously done for bacteriorhodopsin.[13] Multiple scattering has been shown to be very small for such thin crystals.[14]

The unrefined model of the tubulin dimer (PDB ID 1TUB) was first refined as two rigid bodies

which resulted in a crystallographic *R*-factor of about 42.0. Several cycles of maximum-likelihood incorporating experimental phase information, simulated annealing, positional refinement, constrained temperature refinement and manual rebuilding using O, greatly improved the phase-combined $2F_o - F_c$ density and the *R*-factors (final *R*-factor: 23.2, R_{free}: 29.7). Torsion angle refinement did not improve convergence significantly, so classical Cartesian refinement was used. A major drop in *R*-factors was observed when anisotropic overall temperature factors were used. This is due to the problem of imperfect specimen flatness which causes amplitudes to fall off faster in the direction perpendicular to the crystal plane than parallel to the plane [15] (temperature factors: $B_{11} = 26.54$ Å^2, $B_{22} = 10.8$ Å^2, $B_{33} = -37.35$ Å^2, the last corresponding to the direction perpendicular to the crystal plane). Difference maps and $2F_o - F_c$ maps were calculated using F_{calc} values in place of missing F_{obs} in the missing cone, a necessary step that introduced some model bias.

A number of register errors in the starting model were removed in this process. A magnesium ion was placed in the N-site in a position similar to that of magnesium in other nucleotide binding proteins and the FtsZ:GMPCPP crystal structure (S. C. Cordell and J.L., unpublished results). A large difference peak at the lateral interface was interpreted as a zinc ion. Further improvement of the *R*-factors was achieved by careful optimization of cell constants *a* and *b*. A procedure was used in which several cycles of rigid body refinement and positional minimization were performed for one dimensional scans of cell constants *a* and *b*, monitoring R_{free}. The clear minimum of this search was confirmed by greatly improved bond length averages of the final model when compared to standards derived from small molecule structures of amino acids and derivatives.[16]

Overall the refined structure represents a substantial improvement as judged by geometry statistics and crystallographic *R*-factors. In Figure 1 the excellent fit of the refined model within the $2F_o - F_c$ map shows a clear improvement with respect to the fit of the initial model in the raw density (See Figure 2 in Nogales *et al.*[4]). Most importantly, refinement has corrected numerous ''bad'' bond angles and several significant steric clashes that were present in the original, unrefined model. Essentially all of the structure now falls within the ''allowed'' regions of a Ramanchandran plot, except for loop regions that are poorly defined (residue statistics obtained with PROCHECK [17]). While the Ramachandran plot is still not as good as those for typical high-resolution

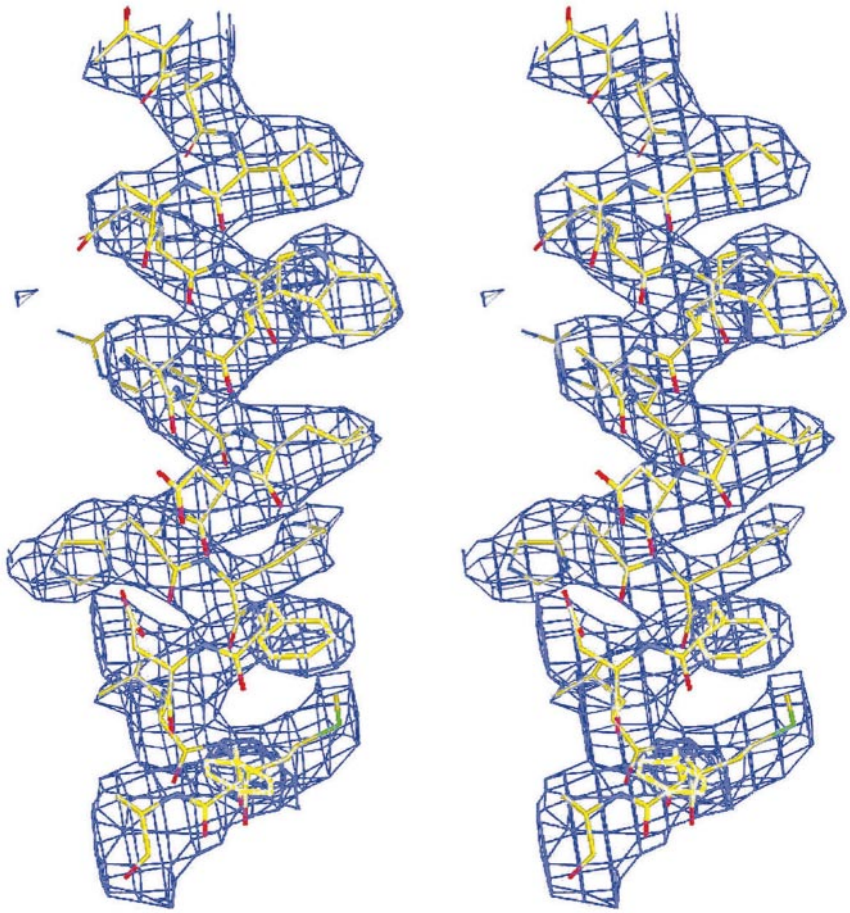

Figure 1. Stereo view of part of the $2F_o - F_c$ map (contoured at 1 σ) and the refined structure of helix H11. The Figure was generated with O.[45]

crystal structures, it compares well with those from other X-ray structures at comparable resolution.[18]

Discussion

Refinement

The crystallographic refinement and manual rebuilding resulted in *R*-factors that are comparable to those for X-ray protein structures of this size and at this low resolution. The *R*-factor of 23.2 and R_{free} of 29.7 are the lowest yet reported for a protein structure determined by electron crystallography (previous values include an *R*-factor of 28 for bacteriorhodopsin (bR),[13] 33.0 and 37.9 (*R*-factor and free *R*-factor) for the green plant light harvesting complex (LHC-II) [19] and 39.9 and 41.7 for aquaporin (AQP-1:[20] for this protein the data set used for the refinement included very low (96 Å) resolution data). Electron crystallographic amplitudes have a much lower signal to noise ratio than typical X-ray data, as judged by Friedel and merging R-factors (Table 1). The large electron crystallography R-factors have thus been attributed to the lower accuracy in determining amplitudes. Major contributors to the low *R*-factors in this work are certainly anisotropic temperature factor correction and bulk solvent correction. Two additional factors are near local symmetry introduced by the very similar structure of α and β-tubulin, and the high solvent content introduced by sampling along *c* in 90 Å intervals. The solvent content is about 70%. Both factors introduce artificial coupling between the amplitudes which keeps the R_{free} closer to the *R*-factor than in a unit cell only filled with random atoms. On the other hand, chemical bonding effects are known to increase *R*-factors at low resolution in electron crystallography, and it has been proposed that a significant part of the high reported *R*-factors is attributable to such effects.[21] Attempts to take bonding effects into account[13,22] have suggested that the *R*-factors could be improved at low resolution and that useful information about charge states could be obtained by including the effects in computation of structure factors from an atomic model. No attempt has been made here to account for bonding effects as aside from an increased *R*-factor at low resolution, they should not significantly affect construction of the model within the density map. However, the large increase in scattering amplitude at low scattering angles for positively charged species probably contributes to our ability to identify the magnesium and zinc ions.

Table 1. Electron crystallographic data and refinement

A. *Two-dimensional crystals*	
Layer group	$P12_1$
Unit cell (refined) (Å)	$a = 81.2$, $b = 93.5$
Thickness (Å)	$c = 90$ (assumed)
B. *Electron diffraction*	
Number of diffraction patterns	208
Resolution (Å)	3.5 (in plane) 4.0 (out of plane)
$R_{Friedel}$ (%)	19
R_{merge} (%)	25
$I/\sigma I$	5.4 (2.3 from 3.7 to 3.5 Å)
Fourier space sampled (%)	84.7
C. *Images*	
Images used	149
Average phase residual	35° (46° from 4 to 3.7 Å)
Fourier space sampled (%)	73
D. *Crystallographic refinement*	
R-factor (20 Å to 3.5 Å) (%)	23.2
Free *R*-factor (20 Å to 3.5 Å) (%)	29.7

During refinement, the *R*-factor decreased from 42.0 to 23.2. A similar measure, R_{phase}, can be calculated as a measure of the difference between calculated and experimental phases, and has been found to be a relevant parameter for electron crystallography. In the course of refining the bacteriorhodopsin structure R_{phase} decreased from 64° to 58°.[13] In refining the tubulin structure R_{phase} actually increased from an initial value of 50.3° to a final value of 54.0°, probably indicating that the original model was fitted accurately into the experimental density, but that the density must have been biased by small errors in the experimental phases.

Electron crystallography is limited in the ability to obtain a complete set of structure factors. The maximum tilt angle of 60-70° for the specimen holder produces a ''hollow cone'' within which data is inaccessible. With a tilt range up to 60°, though, only about 13% of the data is missing. There is thus only a small anisotropy in the point spread function, and with sufficiently high resolution there is no ambiguity in interpretation of the density map.[23] However, a more serious problem arises in practice when specimens are not perfectly flat, causing a loss of signal perpendicular to the tilt axis with tilted specimens. Use of anisotropic temperature factors has reduced the impact of this problem to some extent, but this has, in fact, been the main resolution limit for both phases and amplitudes in the direction perpendicular to the crystal plane.

Regions of major changes

The refined structure has the same overall fold as that obtained originally (Figure 2(a)), a tribute to the quality of the experimental phases. The refinement has allowed a much better definition of side-chain positions, particularly in polar residues on the surface of the molecules. The RMS deviation between the original and refined C^{α} atoms is 2.4 Å when including the long loop near the N terminus of β-tubulin, and 1.6 Å if this retraced loop is ignored (Figure 2(b) shows the original and the retraced loop between H1 and S2 in β-tubulin).

There are small changes in the delimitation of secondary structure, which are not identical for the α and β subunit (Figure 3(a)), and generally corre-

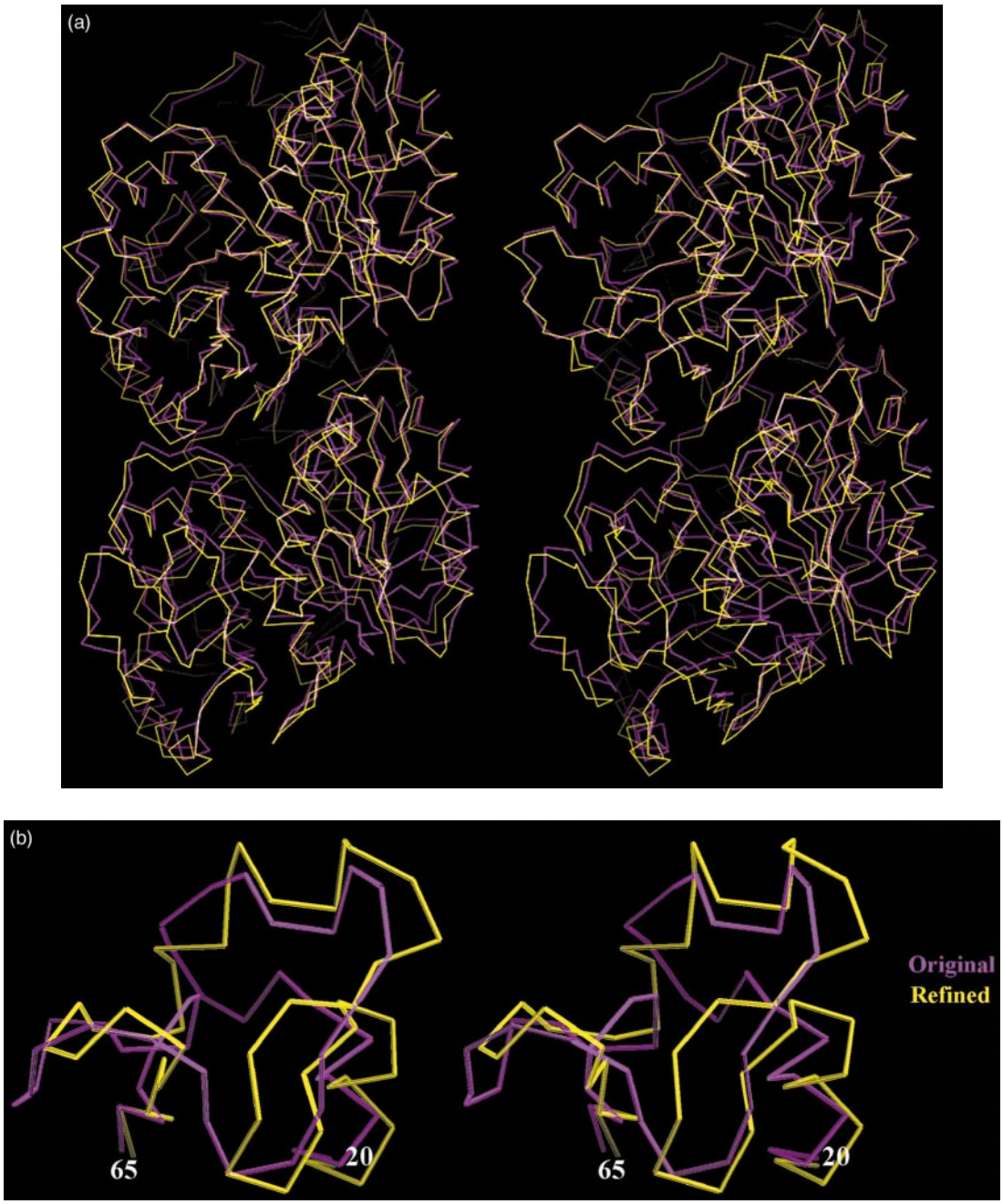

Figure 2. (a) Stereo view of the C^{α} carbon traces for the original model (1TUB, magenta) and the refined model (1JFF, yellow). The stretch in the lattice parameters for the refined model is clearly apparent in this superposition. (b) Stereo view of the retraced loop between H1 and S2 in β-tubulin. The Figure was generated with O.[45]

spond to the appearance of new small helices (H1′, H2′, H2″, H3′, H9′ and H11′). It is not clear whether we can interpret the small differences between α and β-tubulin as significant, or if they are just due to inaccuracy given the limited resolution. It is however interesting to notice that main differences are localized in loop T2 (H2′ and H2″), the structural equivalent of the Switch I region in classical GTPases (Figure 3(b)). Furthermore, helix H3′ is a π-helix in β-tubulin in the present refined model, and thus ''unwound'' with respect to the same helix in α-tubulin. This region in α and β-tubulins corresponds to the Switch II region in classical GTPases. Thus it is tempting to speculate that these small differences reflect the differences in nucleotide state between the two tubulin subunits in the model.

The major changes in the structure of the αβ-tubulin after refinement include three one residue protein sequence frame shifts for both subunits and the retracing of more weakly defined loops. The three protein sequence frame shifts of one residue were detected in identical positions of α and β-tubulin, involving the following residues: 81-97

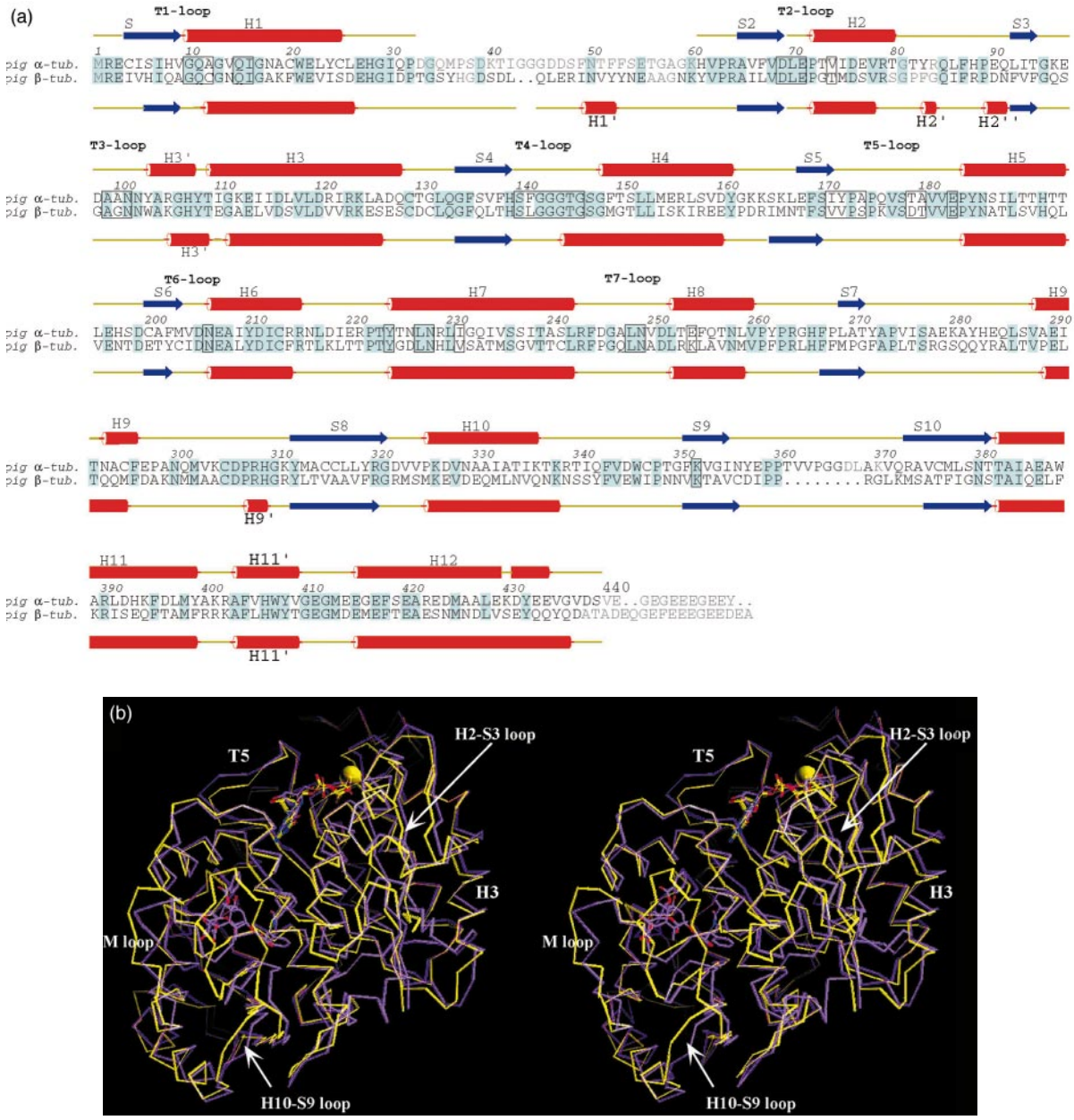

Figure 3. Comparison of the refined structures of α and β-tubulin. (a) Secondary structure for α and β-tubulin in the refined model as defined by dssp.[46] Conserved residues are boxed in blue. New α-helical segments have been labeled with ′ and ″ and the number of the preceding helix. Boxed residues make direct contact with the nucleotide or the magnesium ion. (b) Stereo view of the C^{α} atoms for the refined structures of α (yellow) and β-tubulin (purple). The Figure includes nucleotides and taxol bound to β-tubulin. The Figure was generated with O.[45]

(83-97 in β-tubulin), which include strand B3; 175-197, which comprises loop T5 and helix H5; and 400-405 (now identified as α-helix H11′), between the C-terminal H11 and H12 helices.

As for the initial model, the refined structure lacks the C-terminal tails of both α and β-tubulin. These highly acidic segments are the main site of variability between isotypes and also the main site for posttranslational modifications.[24] Although the mixtures of several different isotypes and posttranslational modifications in bovine brain tubulin (the tubulin source used for the crystallographic studies) may have contributed to the lack of density in the map, it is generally believed that these regions are extended and disordered in microtubules,[25] and most likely also in zinc-induced sheets.[26]

The poorest density area for both α and β-tubulin is located in loop H1-B2 near the N terminus. In the case of α-tubulin the refinement did not result in an improvement of the density, but rather a disappearance of part of it. Consequently residues 35-60 are not included in the model of the α-tubulin. Some improvement was, however, visible for the

β-subunit and this part of the structure is now rebuilt. The path of the polypeptide chain is distinctively different from that previously presented in the unrefined model and includes a small α-helix (H1′). Certain residues still have very poor or almost disconnected density, including His37, Gly38, Ala56, Ala57 and Gly58. The density is also very poor for residues 80-84 (H2-S3 loop) in both α and β-tubulin models.

Several of the other loop regions have been improved substantially. The M-loop, involved in lateral contacts between the protofilaments both in zinc-induced sheets and microtubules, has been retraced. In α-tubulin the B9-B10 loop (residues 363-368), containing an eight residue insertion with respect to β-tubulin, has also been retraced, but densities remain poor for residues Asp367, Leu368 and Lys 370. Although all but one of the loops in the tubulin dimer could be traced, the limited resolution and the anisotropy of the data have resulted in poor Ramachandran plots in some of these loops.

Two important additions to the original model are the inclusion of one magnesium ion at the nucleotide N-site and one zinc ion at the lateral contact between α-subunits. While the existence of the N-site magnesium was expected from numerous experimental results,.[27-29] the accuracy of the position of this atom is limited due to the anisotropy of the density map. In the α-subunit an extra density adjacent to the M-loop has been tentatively assigned to a zinc atom that contributes significantly to the contact and to the stabilization of the M-loop. The identification and positioning of the zinc ion is slightly more speculative. However, both the size and the residues surrounding the density attributed to Zn^{2+} agree well with this assignment.

Sequence conservation and tubulin polymerization

The high conservation of the αβ-tubulin sequences across species has been interpreted as a consequence of the restrictions imposed by tubulin self-assembly. Mutation of a residue in a surface involved in tubulin-tubulin contacts could dramatically affect polymerization unless a number of coordinated mutations were to occur simultaneously across the interface to compensate for the deleterious effect. It is most interesting how this hypothesis is ratified by the present tubulin model. The larger stretches of absolutely conserved residues (taken from Burns & Surridge[30]) cluster in a well defined area across the longitudinal interface between tubulin subunits. This region corresponds to the T3 loop and the loop and small helix H11′ between H11 and H12, on one side, and helix H8 on the other. This region is particularly well defined in the electron density map and thus the accuracy of this part of the α and β-tubulin chains is especially good. In contrast, residues involved in lateral contacts cluster in regions of divergence between species and marked differences between α and β-tubulins. This suggests that both variability in protofilament numbers and, most generally, marked differences in dynamic instability, seem to be obtained by variations in residues involved in contacts between protofilaments.

Monomer stability

Tubulin is particularly rich in aromatic residues. A series of aromatic residues contribute to the stability and robustness of the nucleotide binding domain as they align and stack against each other in the beta sheet (Figure 4).

Of particular interest is the region of contact between the N-terminal and the second domain in β-tubulin. A relative rotation of these domains has been proposed to be linked to microtubule depolymerization following nucleotide hydrolysis.[31] Essential to this interface are residues 198 to 216 including strand S6 and helix H6. This section of the N-terminal domain interacts with the core helix H7, and with several regions in the intermediate domain, specially strand S7 and the long loop following helix H9. Of particular interest is β:Tyr202. The side-chain hydrogen bonds to Asn167 and Glu200 in an otherwise very hydrophobic region. In α-tubulin the tyrosine is substituted by a phenylalanine that makes non-polar interactions with Leu167 and Cys200. In fungi β-tubulin also has a phenylalanine at position 202, and accordingly residue 167 is an alanine while there is no consensus for position 200. In *Saccharomyces cerevisiae* mutation of Glu200 to alanine results in benomyl resistance,[11] suggesting that such change results in impaired drug binding or, more likely, in a gain in microtubule stability. Interestingly, Antarctic fish β-tubulin have a phenylalanine in position 202, in spite of the conservation of Asn167 and Glu200.[32] Microtubules from these species are cold resistant and have reduced dynamics, further suggesting the importance of this region in the stability of microtubules *via* its role at the domain boundary in β-tubulin.

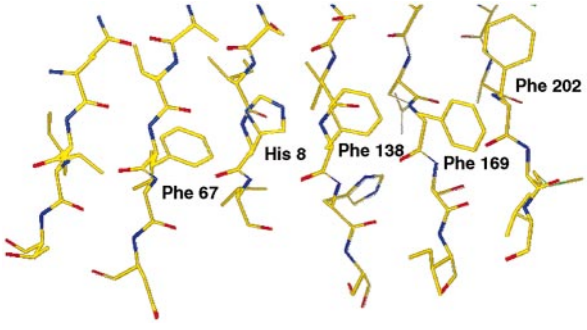

Figure 4. Stacking of aromatic residues in the N-terminal β-sheet of α-tubulin. The Figure was generated with O.[45]

Nucleotide binding

The conformation of the nucleotide and binding pocket in both α and β-tubulin have improved with the refinement (Figure 5). Residues directly in contact with the nucleotide have been boxed in Figure 3. The specificity of tubulin for GTP is obtained by the hydrogen bonding of the 2-exocyclic amino group in GTP to the hydroxyl groups of Asn206 and Asn228, and by hydrogen bonding of the 6-oxo group to the amino group of Asn206. These interactions are in good agreement with predictions based on affinity binding experiments.[33] Otherwise, the base sits in a rather hydrophobic pocket defined by Ile16, Val131, Leu227 and Val231 on one side and Tyr224 on the other. The ribose group interacts with main chain and side-chain groups in the T5 loop, while interaction with the phosphates is dominated by hydrogen bonds with the main chain amines in T1 (the equivalent of the P-loop in G proteins) and T4 (the glycine-rich, tubulin signature motif).

Generally residues involved directly in nucleotide binding and hydrolysis are highly conserved between α and β-subunits, with some interesting exceptions. Residue α:Ala12 is β:Cys12; residue α:Val74 in H2, involved in phosphate binding, is substituted by β:Thr74; residue α:Phe141 in the glycine-rich T4 loop, is substituted by a β:Leu141. The sugar-binding T5 loop is very different for α and β-subunits, with α:Ile171, Tyr172, Pro173, Ala174, Thr179 and Ala180, being substituted in β-tubulin by Val171, Val172, Pro173, Ser174, Asp179 and Thr180. The most significant change between the N-site and E-site is at position 254 in H8, which is a Glu in α-tubulin and a Lys in β-tubulin. Most of these residues, particularly those in T5, are involved in longitudinal contacts between subunits and these difference are probably important for the relative strength and the reversibility of the monomer-monomer and dimer-dimer contacts, as well as the difference in nucleotide hydrolysis in the two regions. While Asp254 in α-tubulin is in an ideal position to be involved in the hydrolysis of the E-site nucleotide, Lys254 in β-tubulin is likely to strengthen the monomer-monomer contacts through its interaction with the phosphate groups of the N-site nucleotide. In addition to this very significant difference, other sequence differences between α and β-tubulin may contribute to the added stability of the intradimer *versus* the interdimer contacts. In particular there are a number of hydrophobic residues at the intradimer interface that are hydrophilic for the dimer-dimer contact: β:Ile347 (*versus* α:Cys347), β:Val257 (*versus* α:Thr257), or α:100Ala (*versus* β:100Gly). These hydrophobic residues are likely to contribute to the instability of the tubulin monomers.

The overall conservation of residues involved in nucleotide binding and hydrolysis extends to other tubulin isoforms as well as the bacterial homologue FtsZ. Interestingly, there are exceptions where some of those motifs drastically diverge from the consensus. A dramatic sequence deviation concerning a highly conserved tubulin motif occurs for δ-tubulins in loop T7, emphasizing the divergence of this tubulin with respect to the rest. The consensus sequence GxxNxD is changed in δ-tubulins to YxxN-P. The GxxNxD motif is a marker of longitudinal interactions between tubulins and FtsZs. Another striking change occurs in γ-tubulin with a Gly-Gly insertion in the T3 loop preceding a highly conserved sequence within the tubulin family (GNNWAxG). Finally loop T5, involved both in nucleotide-ribose binding and longitudinal contacts along protofilaments, is a region of significant variability in sequence and length among tubulins. This variability is likely to affect the ability of these tubulin isoforms to make longitudinal contacts with other tubulin molecules.[34]

In the refined structure a magnesium ion has been built into extra density at the N-site. No

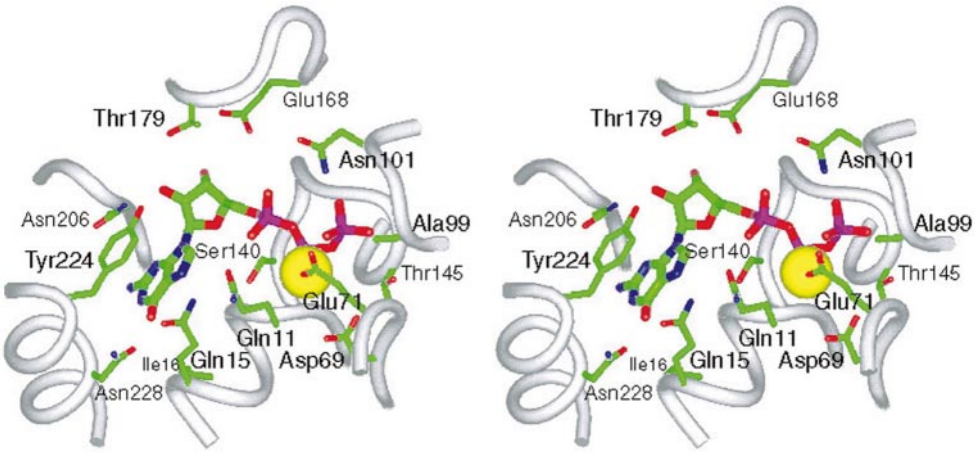

Figure 5. Nucleotide-binding site in α-tubulin with residues involved in direct interactions with the GTP and the magnesium ion. The Figure was generated with Insight II (Biosym Inc.).

equivalent density could be seen at the E-site where the nucleotide has clearly been hydrolyzed. It has been known for a while that GTP-tubulin has two tightly bound Mg^{2+} (at the N- and E-sites), whereas GDP-tubulin has a single high affinity Mg^{2+}.[27] The magnesium ion at the N-site controls the stability and structure of the αβ-tubulin.[29] At the E-site Mg^{2+} is known to be tightly linked to the binding of GTP.[35] Upon polymerization there is a reduction in the Mg^{2+} content of tubulin, indicating its loss during GTP hydrolysis.[36] The present position of the N-site magnesium agrees well with the position of a magnesium atom in the crystal structure of FtsZ bound to a non-hydrolizable GTP analogue (S.C. Cordell and J.L., unpublished results). In tubulin this magnesium ion is bound by salt bridges with two highly conserved residues, Asp69 and Glu71 in the T2 loop.

Taxol binding

The density corresponding to taxol in the $2F_o - F_c$ map is much better defined than for the raw density for the taxane ring, the core of the taxol molecule (Figure 6(a)). Interestingly, the densities for both the 2-phenyl side-chain and the N′ phenyl group remain low through the refinement, suggesting certain mobility of these groups. While variation in the N′ group seem to have little effect on the binding and activity of taxol derivatives, the 2-phenyl side-chain is absolutely required for function.[37] It is thus surprising that this part of the molecule is not more ordered. The refined taxol structure is in a conformation very similar to that

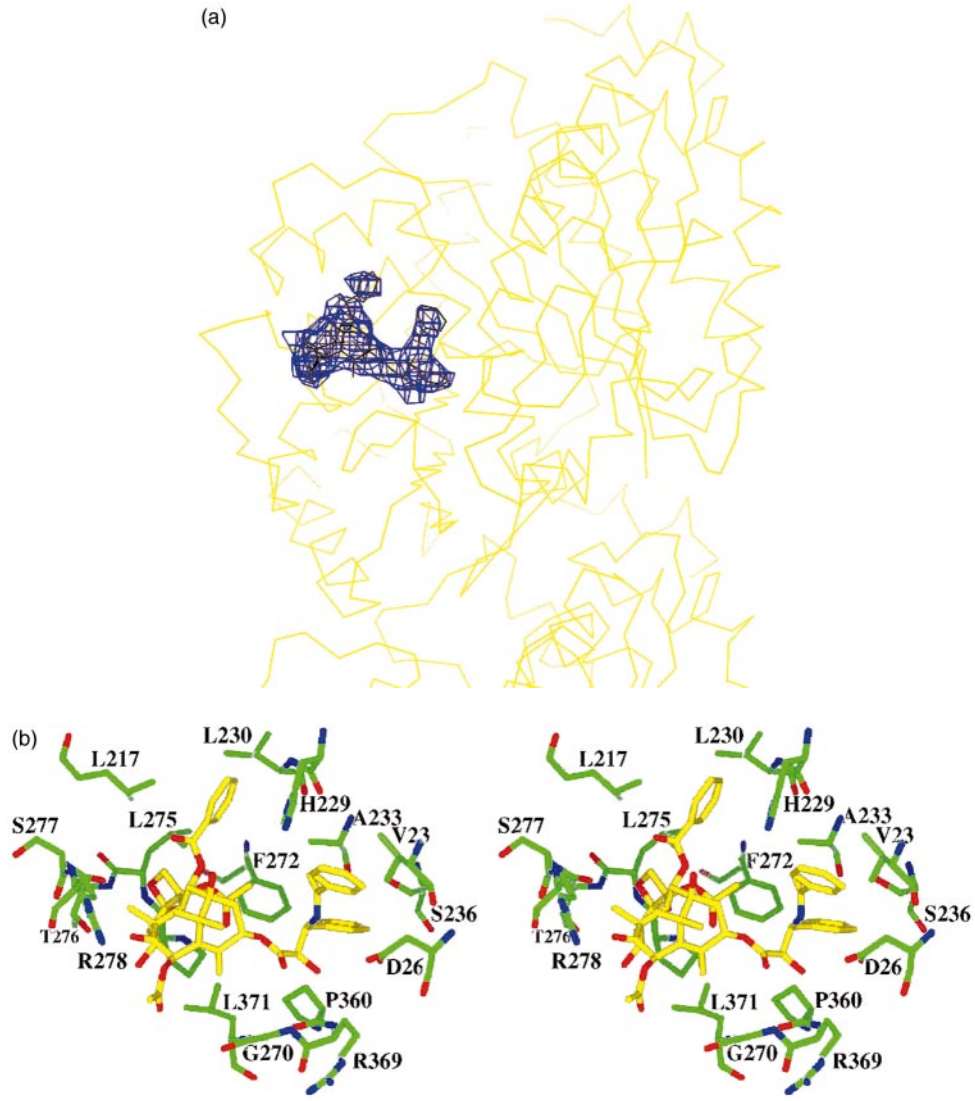

Figure 6. (a) $2F_o - F_c$ density for taxol within the β-tubulin structure shown as C^{α} trace for clarity. The Figure was generated with O.[45] (b) Stereo view of the taxol site including residues that make direct contact with the taxol molecule. The Figure was generated with Insight II (Biosym Inc.).

determined independently by energy-based refinement,[12] except for torsional rotations of the side-chain phenyl rings. In addition, the M-loop of both tubulin subunits has been redrawn, resulting in a slightly different binding pocket.

A considerable number of residues, mostly in the second domain of β-tubulin, are involved in direct contact with the anticancer drug taxol (Figure 6(b)). In helix H1, Val23 makes hydrophobic contact with both the N′ and 3′ phenyl rings, while Asp26 is in hydrogen bonding distance from the nitrogen group in the side-chain. In the H6-H7 loop, Leu217 and Leu219 make hydrophobic contact with the 2-phenyl ring, which is completed by His229 and Leu230 in the core helix (H7). In the same helix Ala233 and Ser236 contact the 3′-phenyl group. The hydrophobic environment of the 3′phenyl group is completed by Phe272 at the end of the B7 strand. Essential for the binding of the taxane ring is the M-loop, in particular residues Pro274, Leu275, Thr276 (which contacts the essential oxetane ring), Ser277 and Arg278. The pocket is completed by residues in the B9-B10 loop (Pro360, Arg369, Gly370 and Leu371).

Lateral contacts

Lateral contacts between protofilaments in the zinc sheets entail extensive interactions between homologous subunits(α-α, β-β). The tightest part of the interface involves the interaction of the M-loop in one subunit with helices H12 and H5 in the adjacent one. H12 has been identified as a major site for interaction of tubulin with motor proteins.[38] The involvement of H12 in lateral interactions in the zinc sheets explains the poor binding of kine-

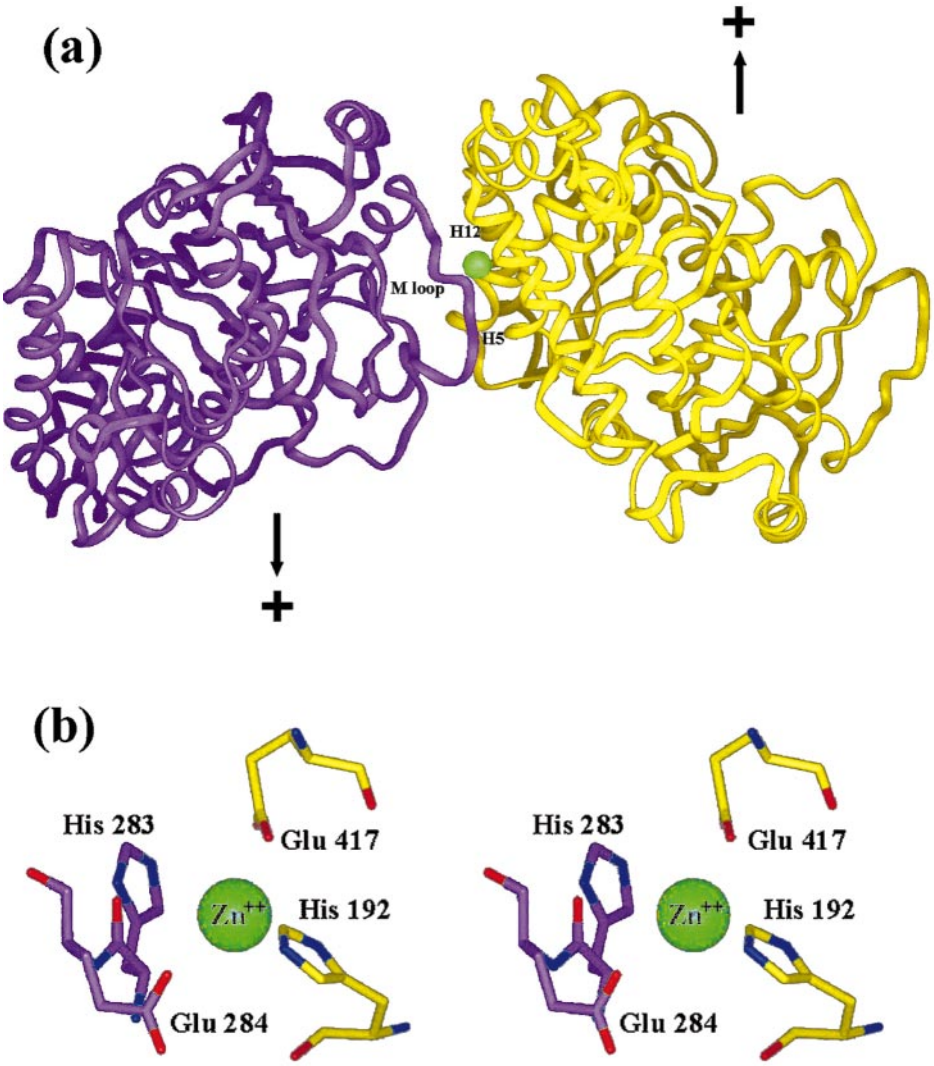

Figure 7. Zinc binding. (a) A putative zinc ion (green) has been modeled at the lateral contacts between α-tubulin subunits, which interacts with the M-loop of the subunit on the left and helices H12 and H5 of the subunit on the right. The arrows point to the plus end of the protofilaments as defined for microtubules. (b) Stereo view of the residues involved in Zn^{2+} binding: His283 and Glu284 on the M-loop, Glu 417 in helix H12 and His192 in helix H5. The Figure was generated with Insight II (Biosym Inc.).

sin-like motors to these polymers, and their destabilizing effect at high concentrations.[39,40]

The lateral contact is more clear between α-subunits as their M-loop is more ordered and thus better defined in the model. In this case, a zinc ion has been modeled into the structure, sitting by residues α:His283, α:Glu284 and α:Gln285 of the M-loop (Figure 7). Residues interacting with the zinc ion at the other side of the interface include α:His192 in helix H5 and α:Glu417 in helix H12, with other acidic residues in H12 also near the site (α:Glu420, α:Glu423 and α:Asp424). His283 and Glu284 are totally conserved residues in α-tubulins (which are substituted by weakly conserved Tyr and Arg in β-tubulins). His192, and all the mentioned residues in H12 are also totally conserved in α-tubulins. The location of zinc and its active, direct participation in lateral interactions strongly suggests that this zinc is as least partially responsible for the generation of the alternative, antiparallel protofilament-protofilament interaction in zinc-induced polymers. Although this is the only zinc ion we can identify, other zinc ions are probably required for the formation of the sheets, perhaps in lower affinity sites.

The involvement of histidines in the binding of the zinc ion agrees with the low pH (~5.8) required for the formation of the sheets. Interestingly, higher pH of 6.0-6.4 results in the formation of macrotubes[39] by bending of the protofilaments accompanied by a longitudinal shift of adjacent protofilaments.[41] This suggests that one or both of the histidines involved in zinc binding has a pK_a of approximately 6, and the differences between the two zinc-induced polymers has to do with differences in the protonation of one or both of these histidine residues.

Lateral contacts also include the interaction of the last residues in helix H6, helix H9 and the following loop, and H10, with residues in helices H4 and H3 in the adjacent subunit. This contact is mostly polar and ionic, involving the interaction of residues α: Arg214, Arg215 and Asn216 in H6 with residues α:Arg156, Val159, Asp160 and Lys163 in H4; and residues α:Asn293 and Glu297 (in H9 and the following loop) with Arg156. The network of interactions extends, through Asn293, to Lys112 and Asp116 in H3, the latter also within interaction distance from Lys338 at the end of helix H10. These residues are not absolutely conserved across species.

Conclusions

In the refined model of αβ-tubulin two loops essential for protofilament interactions in the microtubule, the M-loop and the loop between H1 and S2, have been retraced. A magnesium ion is now modeled within the N-site of α-tubulin. A zinc ion, essential for the formation of the zinc-sheets used for the crystallographic study, has now been localized at lateral contacts between α-tubulin subunits. Most importantly, the refinement of the αβ-tubulin structure has resulted in a much improved geometry and the correction of three small frame shifts. Therefore, this new structure is a significant improvement from the original model, and most relevant for studies involved with the modeling of drug-binding sites on tubulin and with structural changes in tubulin that relate to dynamic instability.

Materials and Methods

Phases for the initial 3.7 Å model were obtained from 149 images, 86 of which were taken at 55-60° tilt.[4] The phase residual for this data set was 30° or better up to 5 Å resolution, 37° between 4 and 5 Å, and 46° for the highest resolution shell. Initial amplitudes were obtained from 94 electron diffraction patterns, which had an overall Friedel *R*-factor of 19% and an overall R_{merge} of 25%.

The initial PDB entry for the tubulin dimer (1TUB) contained a molecule of taxotere, as obtained by X-ray crystallography, docked as a rigid body into the electron density corresponding to taxol. Before we initiated the refinement procedures of the tubulin dimer, we produced a more accurate model of taxol as described.[12] Briefly, 26 conformers of taxol and taxol derivatives obtained from various structural studies, including X-ray crystal structures, NMR nuclear Overhauser enhancement data, as well as a large number of computer-generated conformers, were fitted into the electron crystallographic density associated with the ligand in β-tubulin. One of the best solutions was optimized in the binding site using restricted low temperature dynamics and force field optimization, keeping the evolving model fully consistent with the experimental density of the tubulin-taxol complex. The uniqueness and reproducibility of the final model were independently tested by removing taxol from the protein, conformationally altering it and flexibly redocking it into the binding pocket. Only two of the generated structures were encased by the protein, and the lowest energy form was identical in shape and location to that previously obtained. This energy-minimized taxol was used as a starting point for the crystallographic refinement.

An experimental figure-of-merit (FOM) for the phases was calculated from the deviation of experimental phases from the curves fit to the measurements.[42] These FOM values proved unsuitable for refinement as they did not improve the convergence of refinement. Instead equally weighted phase probability functions derived from phase angles were used.

Because the amplitude data showed a rather high internal temperature factor when fitted in a Wilson plot (approx 65 Å^2), the amplitudes were sharpened by a temperature factor of −25 Å^2. Five percent of reflections were selected randomly and were used throughout the refinement for the calculation of R_{free}. Phases were converted into unimodal Hendrickson-Lattmann coefficients and blurred by a scale factor of 0.2 and a temperature factor of 50.0. These numbers were found empirically by a two-dimensional optimization of R_{free} after maximum-likelihood positional refinement. Atomic scattering factors for electrons[43] were used without modification and without taking charge or chemical bonding effects into account.

All refinement procedures were carried out in CNS version 0.9.[44]

Protein Data Bank accession numbers

The coordinates described here were deposited at the PDB with accession number 1JFF.

Acknowledgments

This work was supported by NIH grant GM46033 (K.H.D.) and by the Office of Health and Enviromental Research of the U.S. Department of Energy under contract DE.AC03.76F00098 (K.H.D. and E.N.).

References

1. Hyams, J. S. & Lloyd, C. W. (1993). Microtubules. In *Modern Cell Biology* (Harford, J. B., ed.), Wiley-Liss, New York.
2. Mitchison, T. & Kirschner, M. (1984). Dynamic instability of microtubule growth. *Nature,* **312**, 237-242.
3. MacNeal, R. K. & Purich, D. L. (1978). Stoichiometry and role of GTP hydrolysis in bovine neurotubule assembly. *J. Biol. Chem.* **253**, 4683-4687.
4. Nogales, E., Wolf, S. G. & Downing, K. H. (1998). Structure of the αβ tubulin dimer by electron crystallography. *Nature,* **391**, 199-203.
5. Nogales, E., Wolf, S. G., Zhang, S. X. & Downing, K. H. (1995). Preservation of 2-D crystals of tubulin for electron crystallography. *J. Struct. Biol.* **115**, 199-208.
6. Nogales, E., Downing, K. H., Amos, L. A. & Löwe, J. (1998). Tubulin and FtsZ form a distinct family of GTPases. *Nature Struct. Biol.* **5**, 451-458.
7. Nogales, E., Whittaker, M., Milligan, R. A. & Downing, K. H. (1999). High resolution structure of the microtubule. *Cell,* **96**, 79-88.
8. Nogales, E. (1999). A structural view of microtubule dynamics. *Cell. Mol. Life Sci.* **56**, 133-142.
9. Löwe, J. & Amos, L. A. (1998). Crystal structure of the bacterial cell division protein FtsZ. *Nature,* **391**, 203-206.
10. Dai, K., Mukherjee, A., Xu, Y. & Lutkenhaus, J. (1994). Mutations in FtsZ that confer resistance to SulA affect the interaction of FtsZ with GTP. *J. Bacteriol.* **175**, 130-136.
11. Richards, K. L., Anders, K. R., Nogales, E., Schwartz, K., Downing, K. H. & Botstein, D. (2000). Structure-function relationships in yeast tubulins. *Mol. Biol. Cell,* **11**, 1887-1903.
12. Snyder, J. P., Nettles, J. H., Cornett, B., Downing, K. H. & Nogales, E. (2001). The binding conformation of taxol in beta tubulin: a model based on the electron crystallographic density. *Proc. Natl Acad. Sci. USA,* **98**, 5312-5316.
13. Grigorieff, N., Ceska, T. A., Downing, K. H., Baldwin, J. M. & Henderson, R. (1996). Electron-crystallographic refinement of the structure of bacteriorhodopsin. *J. Mol. Biol.* **259**, 393-421.
14. Glaeser, R. M. & Downing, K. H. (1993). High-resolution electron crystallography of protein molecules. *Ultramicroscopy,* **52**, 478-486.
15. Henderson, R., Baldwin, J. M., Ceska, T. A., Zemlin, F., Beckman, E. & Downing, K. H. (1990). Model for the structure of bacteriorhodopsin based on high-resolution eletron cryo-microscopy. *J. Mol. Biol.* **213**, 899-929.
16. Engh, R. A. & Huber, R. (1991). Accurate bond and angle parameters for X-ray protein structure refinement. *Acta Crystallog. sect. A,* **47**, 392-400.
17. Laskowski, R. A., Macarthur, M. W., Moss, D. S. & Thornton, J. M. (1993). Procheck - a program to check the stereochemical quality of protein structures. *J. Appl. Crystallog.* **26**, 283-291.
18. Kleywegt, G. J. & Jones, T. A. (1996). Phi/psi-chology: Ramachandran revisited. *Structure,* **4**, 1395-1400.
19. Kühlbrandt, W., Wang, D. N. & Fuiyoshi, Y. (1994). Atomic model of plant light-harvesting complex. *Nature,* **367**, 614-621.
20. Murata, K., Mitsuoka, K., Hirai, T., Walz, T., Agre, P., Heymann, J. B. *et al*. (2000). Structural determinants of water permeation through aquaporin-1. *Nature,* **407**, 599-605.
21. Chang, S., Head-Gordon, T., Glaeser, R. M. & Downing, K. H. (1999). Chemical bonding effects in the determination of protein structures by electron crystallography. *Acta Crystallog. sect. A,* **55**, 305-313.
22. Mitsuoka, K., Hirai, T., Murata, K., Miyazawa, A., Kidera, A., Kimura, Y. *et al*. (1999). The structure of bacteriorhodopsin at 3.0 angstrom resolution based on electron crystallography: implication of the charge distribution. *J. Mol. Biol.* **286**, 861-882.
23. Glaeser, R. M., Tong, L. & Kim, S. (1989). Three dimensional reconstructions from incomplete data: interpretability of density maps at ''atomic'' resolution. *Ultramicroscopy,* **27**, 307-318.
24. Ludueña, R. F. (1998). The multiple forms of tubulin: different gene products and covalent modifications. *Int. Rev. Cyt.* **178**, 207-275.
25. Sackett, D. L. (1995). Structure and function in the tubulin dimer and the role of the acidic carboxyl terminus. In *Proteins: Structure, Function and Engineering* (Biswas, B. B. & Roy, S., eds), vol. 24, pp. 255-302, Plenum Press, New York.
26. Wolf, S. G., Nogales, E., Kikkawa, M., Gratzinger, D., Hirokawa, N. & Downing, K. H. (1996). Interpreting a medium-resolution model of tubulin: comparison of zinc-sheet and microtubule structure. *J. Mol. Biol.* **263**, 485-501.
27. Correia, J. J., Beth, A. H. & Williams, R. C., Jr (1988). Tubulin exchanges divalent cations at both guanine nucleotide-binding sites. *J. Biol. Chem.* **263**, 10681-10686.
28. Carlier, M.-F., Didry, D. & Valentin-Ranc, C. (1991). Interaction between chromium GTP and tubulin. *J. Biol. Chem.* **266**, 12361-12368.
29. Menendez, M., Rivas, G., Diaz, J. F. & Andreu, J. M. (1998). Control of the structural stability of the tubulin dimer by one high affinity bound magnesium ion at nucleotide N-site. *J. Biol. Chem.* **273**, 167-176.
30. Burns, R. G. & Surridge, C. D. (1993). Tubulin: conservation and structure. In *Microtubules* (Hyams, J. S. & Lloyd, C. W., eds), vol. 1, pp. 3 and 32, John Wiley & Sons, Inc., New York.
31. Amos, L. A. & Löwe, J. (1999). How taxol stabilizes microtubule structure. *Chem. Biol.* **6**, R65-R69.
32. Detrich, H. W., Parker, S. K., Williams, R. C., Nogales, E. & Downing, K. H. (2000). Cold adaptation of microtubule assembly and dynamics - structural interpretation of primary sequence changes present in the alpha- and beta-tubulins of antarctic fishes. *J. Biol. Chem.* **275**, 37038-37047.
33. Chakrabarti, G., Mejillano, M. R., Park, Y. H., Vander Velde, D. G. & Himes, R. H. (2000). Nucleo-

side triphosphate specificity of tubulin. *Biochemistry,* **39**, 10269-10274.
34. Inclan, Y. & Nogales, E. (2001). Potential for self-assembly and microtubule interaction of γ-, δ- and ε-tubulin. *J. Cell Sci.* **114**, 413-422.
35. Correia, J. J., Baty, L. T. & Williams, R. C., Jr (1987). Mg^{2+} dependence of guanine nucleotide binding to tubulin. *J. Biol. Chem.* **262**, 17278-17284.
36. Grover, S. & Hamel, E. (1994). The magnesium-GTP interaction in microtubule assembly. *Eur. J. Biochem.* **222**, 163-172.
37. Kingston, D. G. (1994). Taxol: the chemistry and structure-activity relationships of a novel anticancer agent. *Trends Biotechnol.* **12**, 222-227.
38. Kikkawa, M., Okada, Y. & Hirokawa, N. (2000). 15 Å resolution model of the monomeric kinesin motor, KIF1A. *Cell,* **100**, 241-252.
39. Ray, S., Wolf, S. G., Howard, J. & Downing, K. H. (1995). Kinesin does not support the motility of zinc-macrotubes. *Cell Motil. Cytoskel.* **30**, 146-152.
40. Han, Y., Sablin, E. P., Nogales, E., Fletterick, R. J. & Downing, K. H. (1999). Visualizing a new binding site of ncd-motor domain on tubulin. *J. Struct. Biol.* **128**, 26-33.
41. Wolf, S. G., Mosser, G. & Downing, K. H. (1993). Tubulin conformation in zinc-induced sheets and macrotubes. *J. Struct. Biol.* **111**, 190-199.
42. Amos, L., Henderson, R. & Unwin, P. N. (1982). Three-dimensional structure determination by electron microscopy of two-dimenional crystals. *Prog. Biophys. Mol. Biol.* **39**, 183-231.
43. Doyle, P. A. & Turner, P. S. (1968). Relativistic Hartree-Fock X-ray and electron scattering factors. *Acta Crystallog. sect. A,* **24**, 390-397.
44. Brunger, A. T., Adams, P. D., Clore, G. M., DeLano, W. L., Gros, P., GrosseKunstleve, R. W. *et al*. (1998). Crystallography and NMR system: a new software suite for macromolecular structure determination. *Acta Crystallog. sect. D,* **54**, 905-921.
45. Jones, T. A., Zou, J.-Y., Cowan, S. W. & Kjelgaard, M. (1991). Improved methods of building protein models in electron density maps and the location of errors in these models. *Acta Crystallog. sect. A,* **47**, 110-119.
46. Kabsch, W. & Sander, C. (1983). Dictionary of protein secondary structure: pattern recognition of hydrogen-bonded and geometrical features. *Biopolymers,* **22**, 2577-2637.

Edited by I. A. Wilson

(Received 25 June 2001; received in revised form 30 August 2001; accepted 5 September 2001)